ACS OMEGA

Open Access

http://pubs.acs.org/journal/acsodf

Article

Heterogeneous Acetalization of Benzaldehyde over Lanthanide Oxalate Metal−Organic Frameworks

Reem H. Alzard,* Sara Alsaedi, Seeta Alseiari, Shooq Aljasmi, Hesham F. El-Maghraby, Vijo Poulose, Abdelwahab Hassan, Mohamed Kamel, Aya Ali, M. Abdel-Hafiez, and Mohamed Abdellah*

Cite This: *ACS Omega* 2024, 9, 37386−37395

Read Online

ACCESS | Metrics & More | Article Recommendations | Supporting Information

ABSTRACT: Lanthanides (Ln) from the f-blocks of the periodic table have gained significant interest due to their unique characteristics, including magnetism, photoluminescence, and catalysis. In this study, a series of lanthanide metal−organic frameworks [Ln-MOFs, Ln = Eu(III), Tb(III), Nd(III), Er(III), Ho(III), Gd(III), Pr(III), and Dy(III)] were constructed based on oxalic acid and lanthanide metals as the building blocks. These MOFs were comprehensively characterized using various analytical and spectroscopic techniques, including powder X-ray diffraction, Fourier-transform infrared spectroscopy, thermogravimetric analysis, scanning electron microscopy, energy-dispersive X-ray spectroscopy, nitrogen adsorption−desorption, and Raman spectroscopy. The magnetic properties of the investigated materials were examined, revealing both antiferromagnetic and ferromagnetic interactions within the Ln-Ox MOFs. The catalytic activities of Ln-Ox MOFs were evaluated through the heterogeneous acetalization of benzaldehyde with methanol. Reaction yields by the reported catalysts varied up to 90% depending on the MOF's metal center, and the product was confirmed by gas chromatography−mass spectrometry. Recycling experiments have confirmed the stable regeneration of Ln-Ox MOFs in which the product yields remained the same over four consecutive cycles. The hydrothermal synthesis of these MOFs paves the way for a diverse array of materials showcasing unique lanthanide properties, making them suitable for various applications.

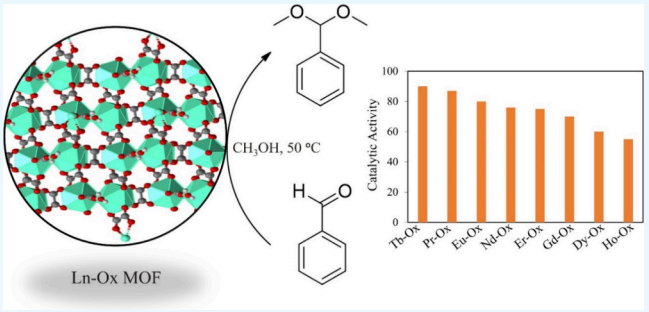

INTRODUCTION

Metal−organic frameworks (MOFs) are leading a new revolution in materials science due to their wide range of applications.[1] The interaction between the metal and the organic linker, as well as the nature of both components, allows for the design of MOFs with anticipated structures for targeted applications such as gas storage and separation,[2,3] catalysis,[4,5] chemical sensing,[6] drug delivery,[7] and light harvesting.[8] The permanent porosity of MOFs is crucial for their catalytic applications, where it can be tuned and altered in a systematic way by employing suitable metal ions and organic ligands. Even more, open-channel MOFs are able to lose/reintroduce the guest species without losing their identity as a framework.,[9] Using metal ions is a common way to generate active catalytic system-based MOFs.[10,11] Lanthanide-based MOFs have attracted increasing attention due to their luminescent, catalytic, and magnetic properties.[12,13] Lanthanide ions tend to coordinate with different organic linkers in variable coordination numbers (6−12) due to their large radius and their partially filled 4f atomic orbitals.

In many organic syntheses, the protection of CO groups is a very important step during the chemical reactions, such as acetalization reactions.[14] Furthermore, the products of acetalization reactions have industrial importance, serving as an ingredient in paints, solvents, and drugs.[15] Due to the increased production of glycerol (a coproduct of biodiesel), benzaldehyde has also been used to produce bioadditives.[16,17] Acetal derivatives were traditionally prepared using strong acids, such as HCl or H_2SO_4 (Brønsted acids). However, these synthesis routes are highly corrosive, produce large amounts of effluents, and require numerous purification/neutralization steps.[6−8] An alternative approach for better catalytic reactions is using heterogeneous acid catalysts, such as graphene oxides,[18] carbon materials,[19,20] montmorillonite,[21,22] zeolites,[23,24] and primarily solid-supported acid dopants such as Amberlyst.[25,26] These are generally matrices with a high-surface-area support, such as silica.[27,28] However, these systems are not easy to fabricate and require post-treatment steps, such

Received: June 20, 2024
Revised: August 5, 2024
Accepted: August 5, 2024
Published: August 21, 2024

as anchoring to the active phase and the thermal post-treatment.[29]

MOFs, as versatile materials, can bestow Lewis and Brønsted acid sites acting as the active catalytic centers in heterogeneous catalysis.[30−32] Recently, different MOFs have been tested on the acetalization of benzaldehyde with methanol since it was first done by an MOF structure reported by Dhakshinamoorthy et al., which had higher catalytic activity for acetal formation compared to zeolites.[33,34] Shortly after, a series of MOFs that are a bit close in design to the UiO-66 MOF was produced by the Timofeeva group in which the relationship of the catalyst acidity and the catalytic activity was studied by varying the linking functional groups on the Lewis acid center of the MOF.[21] According to their results, the enhanced Lewis acidity resulted in a higher catalytic activity in acetalization. In addition to that, it was found out that the Brønsted acid sites generate more essential catalytic activities in acetalization as seen in MIL-100(Cr) and MIL-100(Fe) MOFs.[35] Nevertheless, it is still uncertain whether the Lewis or Brønsted acids determine the catalytic performance of the reaction, even though assorted MOF structures have been employed.[34] Up to now, the limited number of MOFs used for this reaction documented in the literature indicates that the UiO-66(Zr) MOF has superior catalytic acetalization performance.[21,36,37] Notably, only one study by Ren et al. reported the use of a series of lanthanide-based MOFs as catalysts for acetalization in which Tb-MOF achieved the highest product yield after 24 h of the reaction.

Inspired by that, in this study, we have prepared a series of lanthanide-based MOFs using oxalic acid (Ln-Ox) as heterogeneous catalysts for the acetalization of benzaldehyde with methanol, serving as a model reaction. Unlike other materials, lanthanide-based oxalic acid MOFs (Ln-Ox MOFs) are very easy to prepare/activate, contain 1D channels,[38] have high thermal stabilities, and provide the acidic catalytic center (lanthanide centers).[39] The catalytic performances of lanthanide-based MOFs in terms of activity, heterogeneity, and reusability were tested in the acetalization of benzaldehyde with methanol using gas chromatography−mass spectrometry (GC−MS). Our Ln-Ox MOFs show excellent catalytic activity with high reusability.

EXPERIMENTAL SECTION

Materials and Synthesis of Ln-Ox MOFs. Ln-Ox MOFs were prepared as a previously reported procedure.[38] In a typical solvothermal synthesis, 2.5 mmol (315 mg) of oxalic acid was first dissolved in 5 mL of DMF, and 1 mmol of the Ln-nitrate salts (337.98, 435.02, 348.51, 441.02, 438.35, 451.36, 443.35, and 435.01 mg of Eu-nitrate, Tb-nitrate, Dy-nitrate, Ho-nitrate, Gd-nitrate, Er-nitrate, Nd-nitrate, and Pr-nitrate, respectively) was dissolved in 5 mL of deionized water. The metal solution was added dropwise to the linker solution in which the mixture was then capped in a 23 mL Teflon-lined Parr autoclave and placed in a preheated oven at 120 °C for 72 h. Then, the reaction was left to cool to ambient temperature. The obtained products were washed with fresh deionized water and acetone a couple of times before drying and activating them at 120 °C under vacuum for 4 h.

Powder X-ray Diffraction (PXRD). The PXRD diffraction patterns of Ln-Ox MOFs were obtained using a Rigaku MiniFlex benchtop X-ray diffractometer with an excitation source of a Cu Kα radiation tube (λ = 1.542 Å) operating at 40 kV along the range 3−50° 2θ and a rate of 2° min^{-1}.

Fourier-Transform Infrared (FT-IR) Spectroscopy. An Agilent Cary 600 series FT-IR spectrometer with ATR-IR spectroscopy was used to record the FT-IR spectra of Ln-Ox MOFs. The spectral measurements were taken between 4000 and 500 cm^{-1}, and for each spectrum, an average of 512 scans was computed by using a spectral resolution of 2 cm^{-1}. The background spectrum, which was recorded initially, was automatically subtracted from the MOF spectra.

Thermogravimetric Analysis (TGA). Thermal analysis of Ln-Ox MOFs was conducted by a Shimadzu TGA-50 analyzer under nitrogen flow at a rate of 100 mL min^{-1}. The heating flow of the chamber was 5 °C min^{-1} where an aluminum pan holder was used to carry the samples.

Scanning Electron Microscopy (SEM) and Energy-Dispersive X-ray Spectroscopy (EDX). SEM images were taken under high vacuum conditions using an accelerating voltage of 30 kV and a magnification of 5000× with a Quattro SEM instrument equipped with an energy-dispersive X-ray (EDX) for metal composition analysis.

N_2 Adsorption−Desorption. The BET (Brunauer−Emmet−Teller) measurements were conducted through N_2 adsorption−desorption methods on a NOVA touch 2LX within the relative pressure (P/P_o) range of 0.05−1.0, at a temperature of 77.4 K.

Magnetic and Temperature-Dependent Studies. Magnetic measurements were carried out using a Quantum Design Physical Property Measurement System (PPMS) instrument. The temperature-dependent direct-current (DC) magnetization measurements were carried out for samples at an applied field of 1000 Oe. In addition, the variation of DC magnetization as a function of the field was done with an applied field ranging from −70 to +70 kOe at different temperatures.[40,41]

Raman Spectroscopy. Raman spectroscopy was utilized to investigate the vibrational patterns of the Ln-MOFs. The investigations were carried out using a Renishaw inVia spectrophotometer (UK) with an Ar^+ laser excitation source at 514.5 nm. Spectra were recorded within the range of 100−1800 cm^{-1}, with an acquisition time of approximately 10 s. In addition, a 50× objective lens combined with a CCD camera enabled the identification of specific sample regions for spectral examination. This methodology permits the assessment of potential structural or compositional variances across the material's surface.

Catalytic Activity Testing. The catalytic reaction of benzaldehyde acetalization with methanol was performed over Ln-Ox MOF catalysts. Prior to catalytic experiments, the MOFs were further activated in a vacuum oven at 120 °C for around 4 h to ensure that the lanthanide active sites were unsaturated with any trapped solvents or humidity. Then, the activated samples were cooled down to room temperature under a nitrogen atmosphere. Benzaldehyde (0.5 mmol, equivalent to 52 μL) was added to 1.5 mL of methanol (MeOH) where 40 mg of the catalyst was also added. The reaction took place in a capped Pyrex glass vial where the solution was stirred at 50 °C for 12 h. After the reaction completion, the catalyst was washed with MeOH and removed by syringe filtration (except for the recyclable catalyst). The obtained product was then analyzed using GC−MS. The recovered catalyst used for recycling experiments was rinsed with MeOH, dried, and reused with fresh benzaldehyde and methanol for the next run.

https://doi.org/10.1021/acsomega.4c05760
ACS Omega 2024, 9, 37386−37395

Gas Chromatography−Mass Spectrometry (GC−MS). A Shimadzu GC-2010 Plus gas chromatograph equipped with a 30 m × 0.25 mm i.d., 0.25 μm thickness capillary column (RXi-5 Sil) and coupled to a triple-quadrupole detector (GCMS-TQ8040, Japan) was operated with the electron impact (EI) ionization mode at 70 eV. The oven temperature was programmed as follows: starting at 30 °C with a 1 min hold, increasing to 100 °C at a rate of 5 °C per minute with no hold time, and then ramping up to 280 °C at a rate of 10 °C per minute with a 3 min hold. The temperatures for the injector, ion source, and interface were each set to 250 °C. A sample of 5.0 μL was dissolved in 5 mL of methanol, and 0.20 μL was injected in a split mode (1:20) with helium as the carrier gas at a flow rate of 2.0 mL/min. Mass spectra were scanned from m/z 30 to 500. The identification of the analyte was achieved through total ion chromatography (TIC) retention time and by comparing the mass spectra of the identified substance with those of the molecular formulas of individual compounds.

RESULTS AND DISCUSSION

Characterization of Ln-Ox MOFs. PXRD patterns of the activated Ln-Ox samples were investigated to confirm their crystalline structures and phase purities by comparing them to the simulated PXRD patterns[42,43] (Figure 1). The obtained

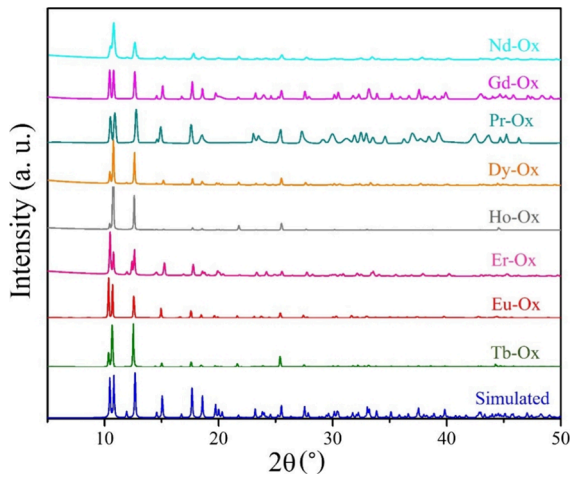

Figure 1. PXRD patterns of the prepared Ln-Ox MOFs compared to the simulated PXRD patterns.

diffraction patterns revealed the successful synthesis of isostructural frameworks with a chemical formula of $[Me_2NH_2][Ln(ox)_2]\cdot 3H_2O$ (Ln = Eu, Tb, Ho, Er, Pr, Dy, and Gd, ox = oxalic acid). All of Ln-Ox MOFs share orthorhombic crystal lattices with unit cell parameters of a = 12.606 Å, b = 12.000 Å, and c = 12.686 Å, which was also confirmed by the literature.[42]

The surface morphologies of Ln-Ox MOFs are shown by the SEM images in Figure 2. Tb-Ox and Eu-Ox exhibit diamond-like crystals of ∼5−10 μm size, while the other MOFs vary in shapes between blocks, plates, or needles. The presence of lanthanide metals within the framework was also evidenced by EDX analysis (Figure S1 and Table S1, Supporting Information).

The solid-state interaction and the binding mode of oxalic acid with Ln metals were confirmed by using FT-IR spectroscopy (Figure 3). The spectrum of the organic linker was compared to the prepared MOF where the carboxylic acid band was clearly shifted to a lower wavenumber (1656 cm^{-1} for oxalic acid to 1618, 1919, 1626, 1625, 1626, 1619, 1627, and 1619 cm^{-1} for Eu-Ox, Tb-Ox, Gd-Ox, Dy-Ox, Nd-Ox, Ho-Ox, Er-Ox, and Pr-Ox MOFs, respectively). This indicates the coordination interaction between the carbonyl groups and the lanthanide ions. Another shift was also observed at ∼1317 cm^{-1} corresponding to C−O bond stretching. In addition, the shift of the O−C−O band in oxalic acid was significantly shifted from 721 to ∼797−800 cm^{-1} in all Ln-Ox MOFs as it is a part of the binding site, which is further evidenced on the chelation of the carboxylate groups to the metal sites. On the other hand, the C−C bond of oxalic acid (at 1380 cm^{-1}) remains intact in all the FT-IR spectra.

Raman spectroscopy was used for the assessment of potential structural or compositional variances across the material's surface. All of the vibration bands obtained for free oxalic acid ($C_2H_2O_4\cdot 2H_2O$) as well as the different MOFs were identified. Figure 4 (black line) shows the vibration bands of free oxalic acid. The vibration at 863 cm^{-1} corresponds to the in-plane bending for δ(C−C) and symmetric stretching for υ(C−O). The peak at 478 cm^{-1} was observed for δ(C−C−O) + δ(C−C). Across all MOF samples, the C═O and C−C−O peaks were observed with weak intensity and slight shifts because of new lanthanide−oxygen bonds.[44] Furthermore, the appearance of a peak at 207 cm^{-1} for υ(Ln−O) confirmed the MOF formation for all samples.

The TGA profiles of Ln-Ox MOFs were obtained from 25 to 600 °C under a N_2 atmosphere. All the prepared materials have shown similar thermal weight loss behavior. As indicated by Figure 5, a weight loss of up to 20% is observed in step (1) at around 100 °C, which is attributed to the loss of water molecules trapped within the frameworks. In the following step (2), starting from 340 °C, a significant weight loss had occurred, which corresponds to the total decomposition of the organic moieties of the MOF lattices (oxalic acid linkers). The formation of a body-centered cubic form of Ln_2O_3[38] was a result of the decomposition of the MOFs, which was also physically observed through the change of color in each Ln-Ox MOF.

N_2 adsorption−desorption measurements were conducted in which Ln-Ox MOFs exhibited type IV isotherms (Figure 6). Surface areas of Ln-Ox MOFs were measured by BET analysis ranging between 5.92 and 11.99 m^2/g. It is worth mentioning that those materials exhibit low surface areas compared to classical MOFs; however, this could be because of oxalic acid being a simple and small linker, which limited the extension of the framework. Average pore sizes of Ln-Ox MOFs were measured to be around 5−20 nm, which is typical for mesoporous MOF materials[45] (Table S2, Supporting Information).

Magnetic Studies of Ln-Ox MOFs. In lanthanide MOFs, magnetic studies elucidate the nature of both antiferromagnetic and ferromagnetic interactions.[46−48] Antiferromagnetic interactions occur when neighboring magnetic moments align in opposite directions, resulting in a net magnetization of zero. To gain deeper insights into the magnetic characteristics of all examined Ln-Ox MOF samples, temperature-dependent magnetization measurements at 1000 Oe ranging from 2 to 300 K were conducted. Figure 7 illustrates the zero-field-cooled (ZFC) magnetization data for the samples under applied magnetic fields of 1000 Oe. At elevated temperatures, the magnetization data exhibit a clear behavior, gradually

https://doi.org/10.1021/acsomega.4c05760
ACS Omega 2024, 9, 37386−37395

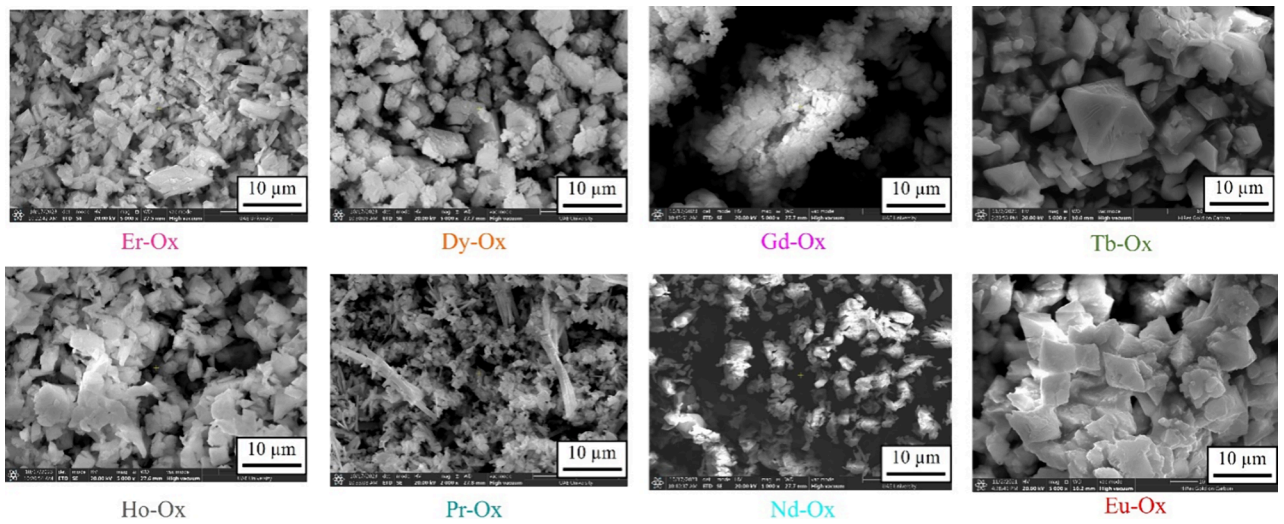

Figure 2. SEM images of Ln-Ox crystals at a 10 μm high resolution.

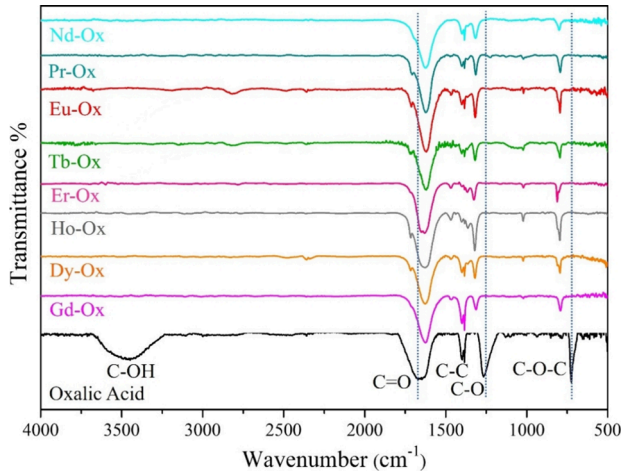

Figure 3. FT-IR spectra of Ln-Ox MOFs compared to the oxalic acid spectrum.

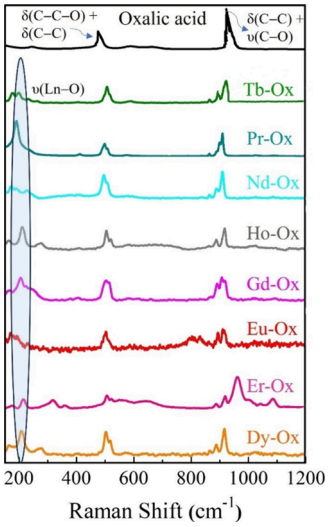

Figure 4. Raman spectra of free oxalic acid and Ln-Ox MOFs.

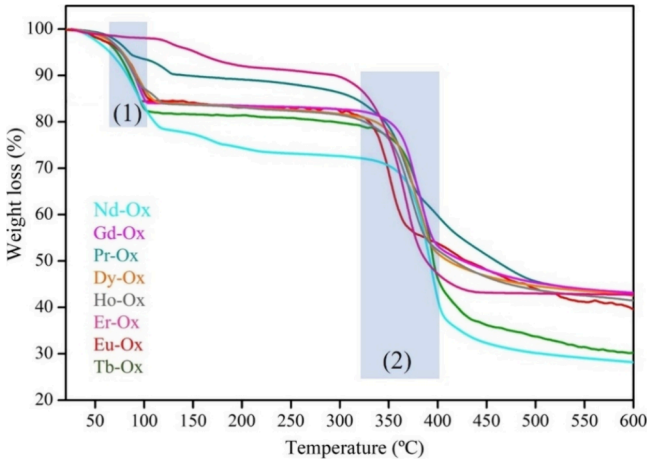

Figure 5. Thermogravimetric analysis of the Ln-Ox MOFs.

increasing as temperature decreases, likely attributed to either localized spin clustering[49] or the growth of ferromagnetic domains.[50] Below a certain temperature dependent on the applied field, the magnetization begins to rise at low temperatures, a phenomenon interpretable in terms of a spin-glass transition or the immobilization of domain wall motion.[51] Throughout the investigated temperature range from 300 to 2 K, the temperature dependence of magnetization consistently diminishes, indicative of antiferromagnetic interactions. This reduction is possibly a consequence of antiparallel coupling between the magnetic moments of neighboring lanthanide ions facilitated by coordination with organic ligands. Further signatures of the possible observed antiferromagnetic behavior are seen from the magnetic hysteresis loop at 2 K (Figure 7). Although the T_c is increasing by changing the rare earth, only a signature of single-phase antiferromagnetic ordering is evident in the temperature dependence (Figure 8). From the M versus H data in Figure 7, an antiferromagnetic type of behavior at 2 and 10 K is observed, while no hysteresis is shown in the inset at 300 K data. Due to the interesting magnetic behavior of these MOFs, a full study of their magnetic properties at different parameters is ongoing and to be published.

Ln-Ox MOF Catalytic Activities. The Lewis acid properties of lanthanide active centers in Ln-MOF catalysts were investigated through an acetalization reaction. As a model substrate, benzaldehyde was selected, and its acetalization with

https://doi.org/10.1021/acsomega.4c05760
ACS Omega 2024, 9, 37386−37395

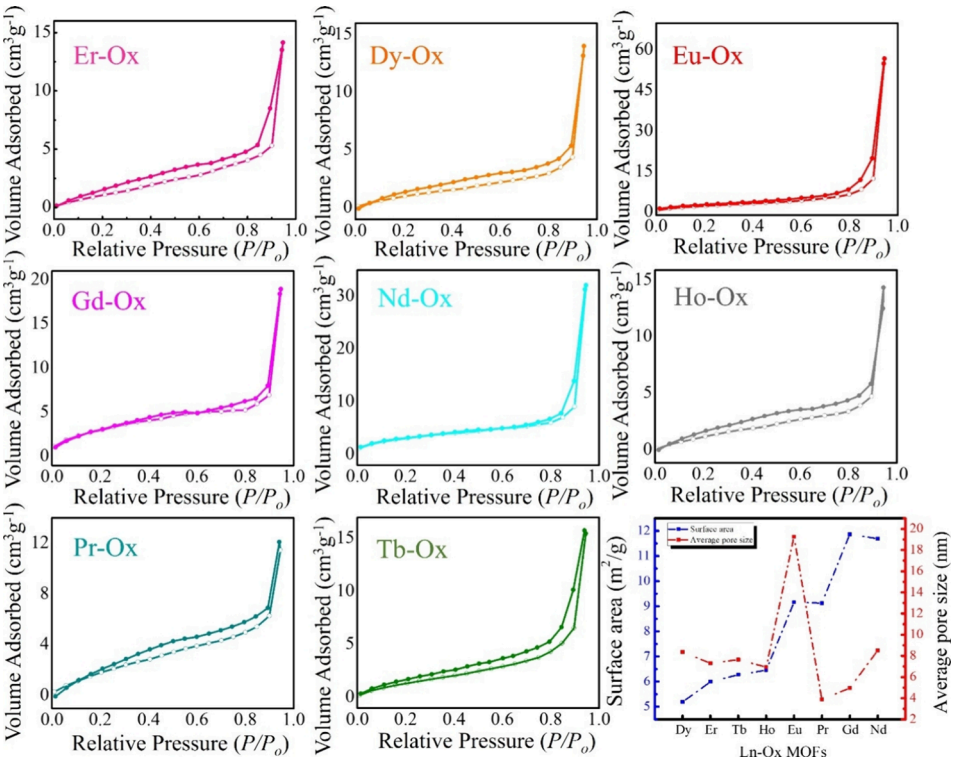

Figure 6. N_2 adsorption−desorption isotherms of Ln-Ox MOF samples and the relations between the surface area and average pore size.

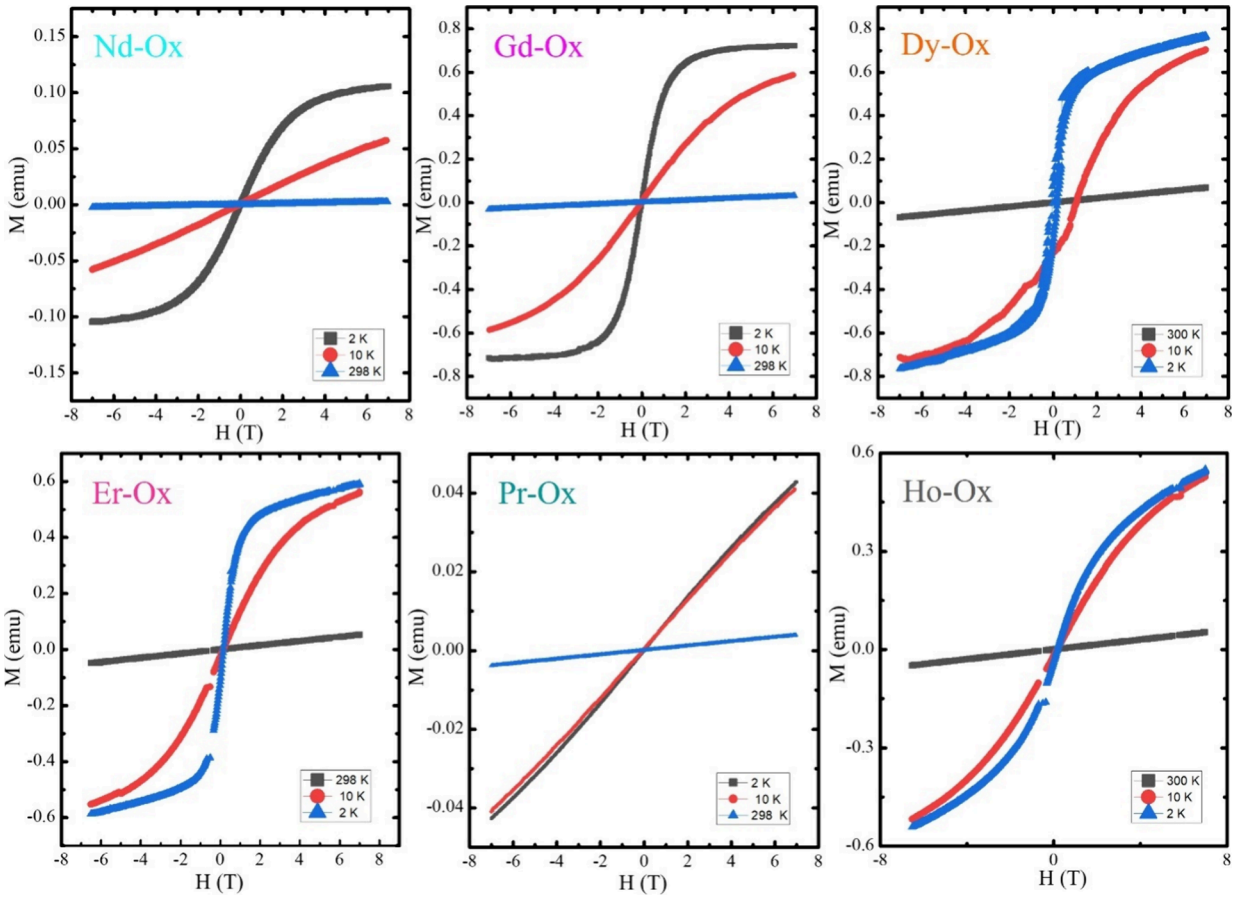

Figure 7. Magnetization vs field isotherms for 2, 10, and 300 K for all investigated samples. The isothermal magnetization plots were measured up to +7 and −7 T.

https://doi.org/10.1021/acsomega.4c05760
ACS Omega 2024, 9, 37386−37395

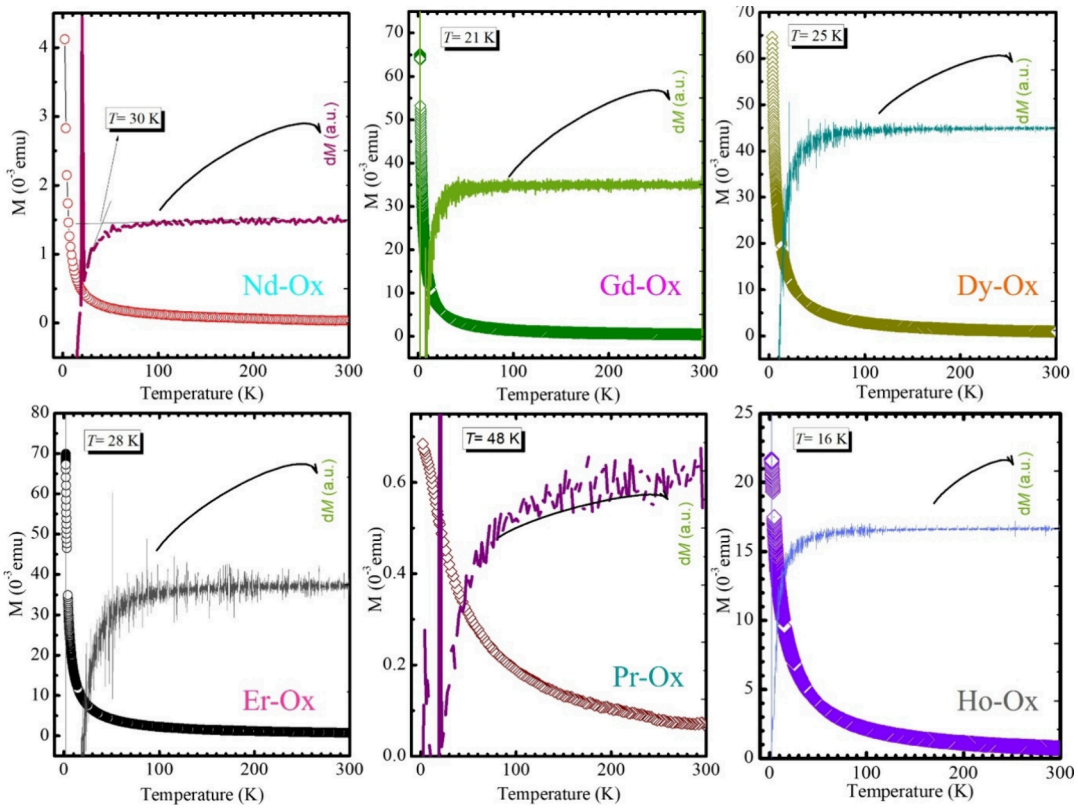

Figure 8. Temperature dependence of magnetization measured under 1000 Oe for all Ln-Ox MOFs.

methanol as a solvent and reagent in the presence of a catalyst was screened. The percentage composition and conversion yields of the reaction components were determined qualitatively by GC−MS (Figures S2 and S3, Supporting Information). This determination was based on comparing the retention times of each component with their respective mass spectra.

The transformation results of benzaldehyde with methanol to (dimethoxymethyl)benzene are summarized in Table 1. Based on our results, the corresponding dimethyl acetal was observed as the major product (≈74%) with each catalytic reaction along with neglectable percentages of benzoic acid (<2%) as a byproduct, which is probably due to the presence of some molecular oxygen.[52] Furthermore, no hemiacetal products were detected, probably because of their unfavorable formation equilibrium.[53] The GC mass spectrum of benzaldehyde at a retention time of 11.3 min revealed a molecular mass peak at m/z = 105 (MW of C_7H_6O, −106.12) (Figure S3a, Supporting Information) accompanied by major fragment ion peaks at m/z = 77 (base peak). For the (dimethoxymethyl)benzene product observed at a retention time of 15.6 min, the mass spectrum displayed a molecular mass peak at m/z = 152 (MW of $C_9H_{12}O_2$, −152.19) along with the major fragment ion peaks at 121 (base peak), 105, 77, and 51, corresponding to the molecular formula $C_9H1_2O_2$ (Figure S3b, Supporting Information). Benzoic acid, a possible side product resulting from the oxidation of benzaldehyde, was detected in small quantities at a retention time 17.09 min with the mass spectrum exhibiting a molecular mass peak at m/z = 122 (MW of $C_7H_6O_2$, −122), with major fragment ion peaks at 105 (base peak), 77, 51, and 32 corresponding to the molecular formula $C_7H_6O_2$.

In catalysis, it is always important to highlight the selectivity, which involves the catalyst's ability to promote favorable reaction pathways, maximizing desired products and minimizing byproducts.[54] For that, we have calculated the selectivity coefficient (α) in terms of the adjusted retention times (t_R) of the starting material and the products (Figure S4, Supporting Information). It was found that the dimethyl acetal product is retained longer than benzaldehyde by a factor of 1.49, indicating a clear separation. Meanwhile, benzoic acid is retained longer than dimethyl acetal by a factor of 1.10, indicating a clear peak resolution. Overall, the selectivity values

Table 1. Acetalization of Benzaldehyde with Methanol over Ln-Ox MOF Catalysts[a]

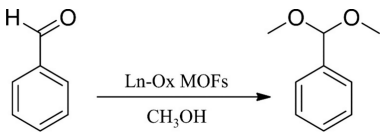

catalyst	conversion (%)[b]	TON[c]	TOF (h^{-1})[d]
Tb-Ox	90 ± 2	4.343	0.362
Pr-Ox	87	4.002	0.334
Eu-Ox	80	3.791	0.316
Nd-Ox	76	8.001	0.294
Er-Ox	75	3.697	0.308
Gd-Ox	70	3.363	0.280
Dy-Ox	60	2.922	0.244
Ho-Ox	55	2.695	0.225

[a]Reaction conditions: benzaldehyde (0.5 mmol), catalyst (40 mg), and methanol (1.5 mL), 50 °C for 12 h. [b]Determined by GC−MS. [c]TON: turnover number = (mmol of the product)/(mmol of the catalyst). [d]TOF: turnover frequency = (mmol of the product)/(mmol of the catalyst) (reaction time, h).

https://doi.org/10.1021/acsomega.4c05760
ACS Omega 2024, 9, 37386−37395

indicate good separation among the starting material, acetalization product, and side product. Each peak is confirmed by both the retention time and mass.

According to Table 1, the highest conversion yield of benzaldehyde was observed over the Tb-Ox MOF with a percentage of 90 ± 2%, while the lowest product yield was observed over the Ho-Ox MOF catalyst. According to the literature and as mentioned in the Introduction, the acidity (Lewis or Brønsted) of the catalytic center is an essential factor for determining the catalytic activity as also explained by previous reports summarized in Table 3. However, there is no specific reason on the variety of conversion yields among similar Ln-based MOF materials used to this kind of reaction. Ren et al., for example, reported a series of Ln-MOFs based on the H_2dpa linker (1,4-phenylenediacetate) where the highest yield was also obtained by Tb-MOF (84%) (entry 7, Table 3) presenting no clear reason on the variety of the conversion yields as well.[53] We speculate that the geometry of the framework could affect the accessibility of the active sites to the substrate. Moreover, the MOF can experience structural changes upon the substrate binding,[55] affecting the catalytic activity; however, there is still no proven evidence on that for these particular Ln-MOFs, and our findings remain inconclusive.

Other catalytic reaction conditions were studied to validate our findings using the Tb-Ox MOF as an example (Table 2). A

Table 2. Control Experiments Carried Out by Tb-Ox MOFs[a]

conditions	conversion (%)[b]	TON[c]	TOF (h^{-1})[d]
40 mg of Tb-Ox, 50 °C	90	4.343	0.362
40 mg of Tb-Ox, no heat	40	1.930	0.161
no Tb-Ox	3	0.145	0.012
5 mg of Tb-Ox	48	2.316	0.193
10 mg of Tb-Ox	51	2.461	0.205
20 mg of Tb-Ox	53	2.557	0.213

[a]Reaction conditions: benzaldehyde (0.5 mmol), catalyst (*x* mg), and methanol (1.5 mL), 50 °C for 12 h. [b]Determined by GC−MS. [c]TON: turnover number = (mmol of the product)/(mmol of the catalyst). [d]TOF: turnover frequency = (mmol of the product)/(mmol of the catalyst) (reaction time, h).

blank control indicated the production of a very small quantity of (dimethoxymethyl)benzene (3%) upon the reaction of benzaldehyde with methanol in the absence of the catalyst, which proves that the acetalization reaction requires a heterogeneous catalyst to occur. In addition, the effect of heat plays an important role in achieving higher product yield in which only a 40% product was yielded at room temperature compared to the reaction at 50 °C. The loading quantity of the catalyst was also studied in which 40 mg was found to be the optimum catalyst loading required to achieve the highest conversion yields compared to lower quantities presented in Table 2 (5, 10, and 20 mg), which is attributed to the availability of more active catalytic sites.

Moreover, recycling experiments were conducted using benzaldehyde and methanol with the Tb-Ox MOF as the catalyst. The reaction was carried out under identical conditions as described earlier. Before being used for the next cycle, the Tb-Ox MOF was washed several times with methanol and separated by centrifugation. The solvent was then decanted, and the sample was dried at 100 °C for 2 h in an oven prior to PXRD measurements. The PXRD patterns of the catalyst were recorded after each cycle where the MOF retained its crystal structure indicating the stability of Ln-Ox MOFs over this reaction (Figure 9). The product conversion

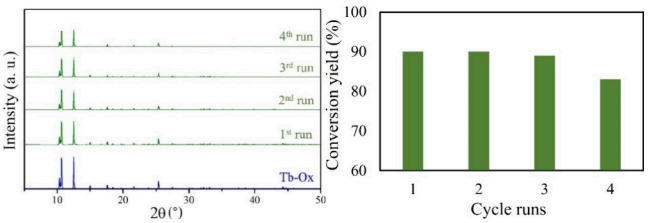

Figure 9. PXRD patterns for the recycled Tb-Ox catalyst with a bar chart of reaction conversion yields.

yield remained the same after three consecutive cycles. However, at the fourth cycle, a decrease in the product yield was observed (83%), which is typical for catalyst performance after the time properly due to the saturation of the active canters within the MOF moieties.[56] Moreover, SEM images were also recorded after the fourth cycle for the Tb-Ox catalyst (Figure S5, Supporting Information), which also shows not much change of the material surface morphology after the catalytic reaction.

Finally, Table 3 summarizes the recent work reported for the acetalization of benzaldehyde and methanol using MOF materials as catalysts for the sake of comparison. Multiple reaction conditions were tested to determine the optimum conditions to achieve the highest product yields. Generally, even though the reaction conditions of all reports are not exactly the same, it is worth noting that our Ln-Ox MOFs have great potential for high catalytic performance, which can be carried out to try other related organic reactions in future work.

Proposed Mechanism for Acetalization using the Tb-Ox Catalyst. As discussed before, there is no clear mechanism or hypothesis for the acetalization reaction of benzaldehyde with methanol. However, the Martos research group has recently reported a plausible mechanism on a Hf-MOF catalyst used for this reaction.[34] This mechanism can be adapted by our Ln-Ox MOFs as hafnium metal has a close nature to lanthanides.[60] It is known that the metal center and the oxygen donors are labile;[59,61] thus, there is a chance for high charge of the metal ion in addition to the fact that lanthanide metals can have multiple coordination vacancies.[47] This is an advantage as it boosts the polarization of a metal−carbonyl bond substrate and promotes deprotonation of the coordinated ROH reagent (methanol molecules). As shown in Scheme 1, it is speculated that the reaction is initiated when the oxygen of benzaldehyde coordinates to the hydrogen atom of the hydroxyl group on the Lewis acid center (lanthanide), which increases the electrophilicity of the carbon in benzaldehyde. Then, a nucleophilic attack occurs between the oxygen atom of methanol and the carbon atom of the carbonyl group of benzaldehyde. Followed by an intermolecular nucleophilic attack by the reaction intermediate, a transfer of a hydrogen atom from the alcohol group to the aldehyde oxygen atom occurs. The carbon of benzaldehyde undergoes another nucleophilic attack by another methanol molecule, which releases an OH group. Finally, a hydrogen atom from the second methanol molecule is bound to the resulting OH, producing a water molecule along with a benzaldehyde dimethyl acetal product where the

https://doi.org/10.1021/acsomega.4c05760
ACS Omega 2024, 9, 37386−37395

Table 3. Summary of Recent MOFs Used as Catalysts for the Benzaldehyde Acetalization Reaction

entry	catalyst	conversion yields (%) (x hour)	reference
1[a]	MOF-808(Zr)	≈95%	34
	MOF-808(Hf)	≈95%	
	UiO-66(Zr)	≈65%	
	UiO-66(Hf)	≈92%	
2[b]	MOF-808 (Zr)-F	≈95% (0.03 h)	57
	MOF-808 (Zr)-S	≈0 (0.03 h)	
3[c]	UiO-66-DES	94 (1 h)	37
	UiO-66-DMF	93 (1 h)	
4[c]	UiO-66-Zr	86, 91, and 83% (0.25, 1, and 24 h, respectively)	36
	UiO-67-Zr	16, 85, and 80% (0.25, 1, and 24 h, respectively)	
5[c]	UiO-66-Zr	50% (4.5 h), 100% (24 h)	58
	UiO-66-NO_2−Zr	100% (6 h)	
6[c]	MIL-101Cr (Cr(BDC))	73% (1 h)	59
7[d]	Ln-MOFs:		53
	$[La_2(dpa)_3]$	<5% (10 h)	
	$[Nd_2(dpa)_3]$	<5% (10 h)	
	$[Eu_2(dpa)_3]$	26% (10 h)	
	$[Yb_2(dpa)_3]$	35% (10 h), 56% (20 h)	
	$[Tb_2(dpa)_3]$	78% (10 h), 84% (20 h)	
8[c]	Fe(BTC)	49% (2 h), 71% (24 h)	33
	$Cu_3(BTC)_2$	63% (2 h), 88% (24 h)	
	$Al_2(BDC)_3$	66% (24 h)	

[a]Reaction conditions: catalyst (0.2 wt %), benzaldehyde (1 mmol), and methanol (37 mmol) at 30 °C. Other conditions were studied. [b]Catalyst (20 mg), benzaldehyde (4 mmol), and methanol (75 mmol, 10 mL) at 30 °C for 0.03 h. [c]Catalyst (50 mg), benzaldehyde (0.94 mmol), and methanol (75 mmol, 3 mL) at room temperature. [d]Catalyst (100 mg), benzaldehyde (1 mmol), and methanol (3 mL) at room temperature.

Scheme 1. Proposed Mechanism of the Acetalization Reaction of Benzaldehyde and Methanol over Ln-Ox Catalysts

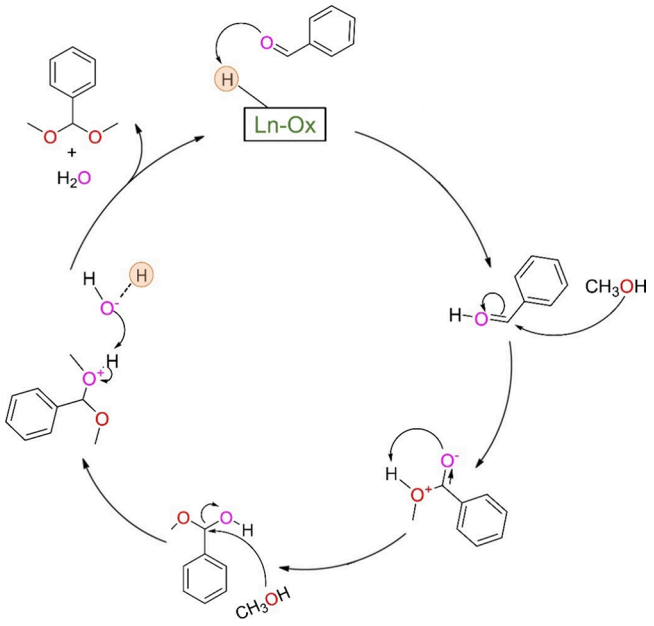

catalyst is recovered.[34] Despite the provided mechanism, it is still challenging to further explore other possible routes of the mechanism and exactly understand the role of the active center as side products such as benzoic acid are also produced by this acetalization reaction.

CONCLUSIONS

We have successfully synthesized a series of isostructural lanthanide-based MOFs using a simple one-pot solvothermal method, all sharing orthorhombic crystal structures. These materials were thoroughly characterized through various analytical, spectroscopic, thermal, and magnetic techniques, revealing their diverse physical and chemical properties. For the first time, Ln-Ox MOFs were employed as efficient heterogeneous catalysts in the acetalization of benzaldehyde with methanol, achieving high product yields, along with remarkable stability and reusability. This study highlights the immense potential of lanthanide-based materials for a broad spectrum of catalytic and magnetic applications, paving the way for future innovations.

ASSOCIATED CONTENT

Supporting Information

The Supporting Information is available free of charge at https://pubs.acs.org/doi/10.1021/acsomega.4c05760.

Characterization of Ln-Ox MOFs (energy-dispersive X-ray spectroscopy (EDX) data and BET analysis of Ln-Ox MOFs) and GC−MS chromatograms (selectivity coefficient calculations and SEM images of the recovered catalyst) (PDF)

AUTHOR INFORMATION

Corresponding Authors

Reem H. Alzard − *Department of Chemistry, UAE University, Al-Ain, UAE*; Email: reem.alzard@uaeu.ac.ae

Mohamed Abdellah − *Department of Chemistry, UAE University, Al-Ain, UAE*; orcid.org/0000-0002-6875-5886; Email: moabdellah@uaeu.ac.ae

Authors

Sara Alsaedi − *Department of Chemistry, UAE University, Al-Ain, UAE*

Seeta Alseiari − *Department of Chemistry, UAE University, Al-Ain, UAE*

Shooq Aljasmi − *Department of Chemistry, UAE University, Al-Ain, UAE*

Hesham F. El-Maghraby − *Department of Chemistry, UAE University, Al-Ain, UAE*

Vijo Poulose − *Department of Chemistry, UAE University, Al-Ain, UAE*

Abdelwahab Hassan − *Physics Department, Faculty of Science, Fayoum University, Fayoum 63514, Egypt*

Mohamed Kamel − *Physics Department, Faculty of Science, Fayoum University, Fayoum 63514, Egypt*

Aya Ali − *Center for Advanced Materials Research, Research Institute of Sciences and Engineering, University of Sharjah, Sharjah, UAE*

M. Abdel-Hafiez − *Department of Applied Physics & Astronomy and Center for Advanced Materials Research, Research Institute of Sciences and Engineering, University of Sharjah, Sharjah, UAE; Physics Department, Faculty of*

https://doi.org/10.1021/acsomega.4c05760
ACS Omega 2024, 9, 37386−37395

Science, Fayoum University, Fayoum 63514, Egypt;
orcid.org/0000-0002-1802-5279

Complete contact information is available at:
https://pubs.acs.org/10.1021/acsomega.4c05760

Notes

The authors declare no competing financial interest.

■ ACKNOWLEDGMENTS

This project was funded by the research office at UAEU [SURE plus 2023 (G00004458) and Research Start-up Proposal (G00004595)]. Authors would like to thank Salama Almeqbaali, Abrar Alkarbi, and Najood Almansoori for their contribution in the synthesis of the MOFs and the Advanced Materials Research Lab at the University of Sharjah.

■ REFERENCES

(1) Yaghi, O. M.; O'Keeffe, M.; Ockwig, N. W.; Chae, H. K.; Eddaoudi, M.; Kim, J. Reticular Synthesis and the Design of New Materials. *Nature* **2003**, *423* (6941), 705−714.
(2) Hasan, Z.; Tong, M.; Jung, B. K.; Ahmed, I.; Zhong, C.; Jhung, S. H. Adsorption of Pyridine over Amino-Functionalized Metal−Organic Frameworks: Attraction via Hydrogen Bonding versus Base−Base Repulsion. *J. Phys. Chem. C* **2014**, *118* (36), 21049−21056.
(3) Li, J.-R.; Kuppler, R. J.; Zhou, H.-C. Selective Gas Adsorption and Separation in Metal−Organic Frameworks. *Chem. Soc. Rev.* **2009**, *38* (5), 1477−1504.
(4) Corma, A.; García, H.; Llabrés i Xamena, F. X. Engineering Metal Organic Frameworks for Heterogeneous Catalysis. *Chem. Rev.* **2010**, *110* (8), 4606−4655.
(5) Zhang, W.; Shi, Y.; Li, C.; Zhao, Q.; Li, X. Synthesis of Bimetallic MOFs MIL-100(Fe-Mn) as an Efficient Catalyst for Selective Catalytic Reduction of NO_x with NH_3. *Catal. Lett.* **2016**, *146* (10), 1956−1964.
(6) Wang, X.; Zhao, J.; Guo, C.; Pei, M.; Zhang, G. Simple Hydrazide-Based Fluorescent Sensors for Highly Sensitive and Selective Optical Signaling of Cu^{2+} and Hg^{2+} in Aqueous Solution. *Sens. Actuators, B* **2014**, *193*, 157−165.
(7) Zheng, H.; Zhang, Y.; Liu, L.; Wan, W.; Guo, P.; Nyström, A. M.; Zou, X. One-Pot Synthesis of Metal−Organic Frameworks with Encapsulated Target Molecules and Their Applications for Controlled Drug Delivery. *J. Am. Chem. Soc.* **2016**, *138* (3), 962−968.
(8) Wang, J.-L.; Wang, C.; Lin, W. Metal−Organic Frameworks for Light Harvesting and Photocatalysis. *ACS Catal.* **2012**, *2* (12), 2630−2640.
(9) Natarajan, S.; Mahata, P. Metal−Organic Framework Structures − How Closely Are They Related to Classical Inorganic Structures? *Chem. Soc. Rev.* **2009**, *38* (8), 2304−2318.
(10) Evans, O. R.; Ngo, H. L.; Lin, W. Chiral Porous Solids Based on Lamellar Lanthanide Phosphonates. *J. Am. Chem. Soc.* **2001**, *123* (42), 10395−10396.
(11) Schlichte, K.; Kratzke, T.; Kaskel, S. Improved Synthesis, Thermal Stability and Catalytic Properties of the Metal-Organic Framework Compound $Cu_3(BTC)_2$. *Microporous Mesoporous Mater.* **2004**, *73* (1), 81−88.
(12) Llabrés i Xamena, F. X.; Corma, A.; Garcia, H. Applications for Metal−Organic Frameworks (MOFs) as Quantum Dot Semiconductors. *J. Phys. Chem. C* **2007**, *111* (1), 80−85.
(13) Rocha, J.; Carlos, L. D.; Paz, F. A. A.; Ananias, D. Luminescent Multifunctional Lanthanides-Based Metal−Organic Frameworks. *Chem. Soc. Rev.* **2011**, *40* (2), 926−940.
(14) Dong, J.-L.; Yu, L.-S.-H.; Xie, J.-W. A Simple and Versatile Method for the Formation of Acetals/Ketals Using Trace Conventional Acids. *ACS Omega* **2018**, *3* (5), 4974−4985.
(15) Tsolakis, N.; Bam, W.; Srai, J. S.; Kumar, M. Renewable Chemical Feedstock Supply Network Design: The Case of Terpenes. *Journal of Cleaner Production* **2019**, *222*, 802−822.
(16) Patel, A.; Pithadia, D. Low Temperature Synthesis of Bio-Fuel Additives via Valorisation of Glycerol with Benzaldehyde as Well as Furfural over a Novel Sustainable Catalyst, 12-Tungstosilicic Acid Anchored to Ordered Cubic Nano-Porous MCM-48. *Applied Catalysis A: General* **2020**, *602*, No. 117729.
(17) Akinnawo, C. A.; Mosia, L.; Alimi, O. A.; Oseghale, C. O.; Fapojuwo, D. P.; Bingwa, N.; Meijboom, R. Eco-Friendly Synthesis of Valuable Fuel Bio-Additives from Glycerol. *Catal. Commun.* **2021**, *152*, No. 106287.
(18) Dhakshinamoorthy, A.; Alvaro, M.; Puche, M.; Fornes, V.; Garcia, H. Graphene Oxide as Catalyst for the Acetalization of Aldehydes at Room Temperature. *ChemCatChem.* **2012**, *4* (12), 2026−2030.
(19) Rodrigues, R.; Gonçalves, M.; Mandelli, D.; Pescarmona, P. P.; Carvalho, W. A. Solvent-Free Conversion of Glycerol to Solketal Catalysed by Activated Carbons Functionalised with Acid Groups. *Catal. Sci. Technol.* **2014**, *4* (8), 2293−2301.
(20) Khayoon, M. S.; Hameed, B. H. Solventless Acetalization of Glycerol with Acetone to Fuel Oxygenates over Ni−Zr Supported on Mesoporous Activated Carbon Catalyst. *Applied Catalysis A: General* **2013**, *464*−*465*, 191−199.
(21) Timofeeva, M. N.; Panchenko, V. N.; Krupskaya, V. V.; Gil, A.; Vicente, M. A. Effect of Nitric Acid Modification of Montmorillonite Clay on Synthesis of Solketal from Glycerol and Acetone. *Catal. Commun.* **2016**, *90*, 65.
(22) Nanda, M. R.; Yuan, Z.; Qin, W.; Ghaziaskar, H. S.; Poirier, M.-A.; Xu, C. A New Continuous-Flow Process for Catalytic Conversion of Glycerol to Oxygenated Fuel Additive: Catalyst Screening. *Appl. Energy* **2014**, *123*, 75−81.
(23) Kowalska-Kus, J.; Held, A.; Frankowski, M.; Nowinska, K. Solketal Formation from Glycerol and Acetone over Hierarchical Zeolites of Different Structure as Catalysts. *J. Mol. Catal. A: Chem.* **2017**, *426*, 205−212.
(24) Roldán, L.; Mallada, R.; Fraile, J. M.; Mayoral, J. A.; Menéndez, M. Glycerol Upgrading by Ketalization in a Zeolite Membrane Reactor. *Asia-Pacific Journal of Chemical Engineering* **2009**, *4* (3), 279−284.
(25) Deutsch, J.; Martin, A.; Lieske, H. Investigations on Heterogeneously Catalysed Condensations of Glycerol to Cyclic Acetals. *J. Catal.* **2007**, *245* (2), 428−435.
(26) Maximov, A. L.; Nekhaev, A. I.; Ramazanov, D. N. Ethers and Acetals, Promising Petrochemicals from Renewable Sources. *Pet. Chem.* **2015**, *55* (1), 1−21.
(27) Tan, X.; Sudarsanam, P.; Tan, J.; Wang, A.; Zhang, H.; Li, H.; Yang, S. Sulfonic Acid-Functionalized Heterogeneous Catalytic Materials for Efficient Biodiesel Production: A Review. *Journal of Environmental Chemical Engineering* **2021**, *9* (1), No. 104719.
(28) Lantos, J.; Kumar, N.; Saha, B. A Comprehensive Review of Fine Chemical Production Using Metal-Modified and Acidic Microporous and Mesoporous Catalytic Materials. *Catalysts* **2024**, *14* (5), 317.
(29) Laguna, O. H.; Lietor, P. F.; Godino, F. J. I.; Corpas-Iglesias, F. A. A Review on Additive Manufacturing and Materials for Catalytic Applications: Milestones, Key Concepts. *Advances and Perspectives. Materials & Design* **2021**, *208*, No. 109927.
(30) Bavykina, A.; Kolobov, N.; Khan, I. S.; Bau, J. A.; Ramirez, A.; Gascon, J. Metal-Organic Frameworks in Heterogeneous Catalysis: Recent Progress, New Trends, and Future Perspectives. *Chem. Rev.* **2020**, *120* (16), 8468−8535.
(31) Guo, J.; Qin, Y.; Zhu, Y.; Zhang, X.; Long, C.; Zhao, M.; Tang, Z. Metal−Organic Frameworks as Catalytic Selectivity Regulators for Organic Transformations. *Chem. Soc. Rev.* **2021**, *50* (9), 5366−5396.
(32) Dhakshinamoorthy, A.; Li, Z.; Garcia, H. Catalysis and Photocatalysis by Metal Organic Frameworks. *Chem. Soc. Rev.* **2018**, *47* (22), 8134−8172.

(33) Dhakshinamoorthy, A.; Alvaro, M.; Garcia, H. Metal Organic Frameworks as Solid Acid Catalysts for Acetalization of Aldehydes with Methanol. *Advanced Synthesis & Catalysis* **2010**, *352* (17), 3022−3030.
(34) García-Rojas, E.; Tapiador, J.; Leo, P.; Palomino, C.; Martos, C.; Orcajo, G. Catalytical Advantages of Hf-MOFs in Benzaldehyde Acetalization. *Catal. Today* **2024**, *434*, No. 114705.
(35) Hall, J. N.; Bollini, P. Metal−Organic Framework MIL-100 Catalyzed Acetalization of Benzaldehyde with Methanol: Lewis or Brønsted Acid Catalysis? *ACS Catal.* **2020**, *10* (6), 3750−3763.
(36) Arrozi, U.; Wijaya, H.; Patah, A.; Permana, Y. Efficient Acetalization of Benzaldehydes Using UiO-66 and UiO-67: Substrates Accessibility or Lewis Acidity of Zirconium. *Applied Catalysis A: General* **2015**, *506*, 77−84.
(37) Chen, L.; Ye, X.; Zhang, T.; Qin, H.; Cheng, H.; Qi, Z. Fast Assembly of Metal Organic Framework UiO-66 in Acid-Base Tunable Deep Eutectic Solvent for the Acetalization of Benzaldehyde and Methanol. *Molecules* **2022**, *27* (21), 7246.
(38) Alzard, R. H.; Siddig, L. A.; Saleh, N.; Nguyen, H. L.; Nguyen, Q. A. T.; Ho, T. H.; Bui, V. Q.; Sethupathi, K.; Sreejith, P. K.; Alzamly, A. A New Mode of Luminescence in Lanthanide Oxalates Metal−Organic Frameworks. *Sci. Rep.* **2022**, *12* (1), 18812.
(39) Zhang, Y.; Liu, S.; Zhao, Z.-S.; Wang, Z.; Zhang, R.; Liu, L.; Han, Z.-B. Recent Progress in Lanthanide Metal−Organic Frameworks and Their Derivatives in Catalytic Applications. *Inorg. Chem. Front.* **2021**, *8* (3), 590−619.
(40) Putilov, A. V.; Di Giorgio, C.; Vadimov, V. L.; Trainer, D. J.; Lechner, E. M.; Curtis, J. L.; Abdel-Hafiez, M.; Volkova, O. S.; Vasiliev, A. N.; Chareev, D. A.; Karapetrov, G.; Koshelev, A. E.; Aladyshkin, A. Yu.; Mel'nikov, A. S.; Iavarone, M. Vortex-Core Properties and Vortex-Lattice Transformation in FeSe. *Phys. Rev. B* **2019**, *99* (14), No. 144514.
(41) Kvashnin, Y.; VanGennep, D.; Mito, M.; Medvedev, S. A.; Thiyagarajan, R.; Karis, O.; Vasiliev, A. N.; Eriksson, O.; Abdel-Hafiez, M. Coexistence of Superconductivity and Charge Density Waves in Tantalum Disulfide: Experiment and Theory. *Phys. Rev. Lett.* **2020**, *125* (18), No. 186401.
(42) Ellart, M.; Blanchard, F.; Rivenet, M.; Abraham, F. Structural Variations of 2D and 3D Lanthanide Oxalate Frameworks Hydrothermally Synthesized in the Presence of Hydrazinium Ions. *Inorg. Chem.* **2020**, *59* (1), 491−504.
(43) Wang, X.; Qin, T.; Bao, S.-S.; Zhang, Y.-C.; Shen, X.; Zheng, L.-M.; Zhu, D. Facile Synthesis of a Water Stable 3D Eu-MOF Showing High Proton Conductivity and Its Application as a Sensitive Luminescent Sensor for Cu^{2+} Ions. *J. Mater. Chem. A* **2016**, *4* (42), 16484−16489.
(44) Morris, D. E.; Hobart, D. E. Raman Spectra of the Lanthanide Oxalates. *J. Raman Spectrosc.* **1988**, *19* (4), 231−237.
(45) Ahmadi, M.; Ebrahimnia, M.; Shahbazi, M.-A.; Keçili, R.; Ghorbani-Bidkorbeh, F. Microporous Metal−Organic Frameworks: Synthesis and Applications. *Journal of Industrial and Engineering Chemistry* **2022**, *115*, 1−11.
(46) Saines, P. J.; Bristowe, N. C. Probing Magnetic Interactions in Metal−Organic Frameworks and Coordination Polymers Microscopically. *Dalton Trans.* **2018**, *47* (38), 13257−13280.
(47) Alzard, R. H.; Siddig, L. A.; Abdelhamid, A. S.; Paz, A. P.; Nguyen, H. L.; Sethupathi, K.; Sreejith, P. K.; Alzamly, A. Lanthanide(Iii) (Er/Ho) Coordination Polymers for a Photocatalytic CO2 Cycloaddition Reaction. *Dalton Trans.* **2023**, *52*, 8473−8487.
(48) Alzard, R. H.; Siddig, L. A.; Abdelhamid, A. S.; Ramachandran, T.; Alzamly, A. Structural Analysis and Photocatalytic Activities of Bismuth-Lanthanide Oxide Perovskites. *J. Solid State Chem.* **2024**, *329*, No. 124359.
(49) Nakamura, S.; Soeya, S.; Ikeda, N.; Tanaka, M. Spin-Glass Behavior in Amorphous $BiFeO_3$. *J. Appl. Phys.* **1993**, *74* (9), 5652−5657.
(50) Vincent, E.; Dupuis, V.; Alba, M.; Hammann, J.; Bouchaud, J.-P. Aging Phenomena in Spin Glass and Ferromagnetic Phases: Domain Growth and Wall Dynamics. *Europhys. Lett.* **2000**, *50* (5), 674−680.
(51) Chang, H.; Guo, Y.; Liang, J.; Rao, G. Magnetic Ordering and Irreversible Magnetization between ZFC and FC States in RCo 5Ga 7 Compounds. *J. Magn. Magn. Mater.* **2004**, *278*, 306−310.
(52) da Silva, M. J.; Ribeiro, C. J. A.; de Araújo, E. N.; Torteloti, I. M. Acetalization of Alkyl Alcohols with Benzaldehyde over Cesium Phosphomolybdovanadate Salts. *Processes* **2023**, *11* (7), 2220.
(53) Ren, Y.; Liang, J.; Lu, J.; Cai, B.; Shi, D.; Qi, C.; Jiang, H.; Chen, J.; Zheng, D. 1,4-Phenylenediacetate-Based Ln MOFs − Synthesis, Structures, Luminescence, and Catalytic Activity. *Eur. J. Inorg. Chem.* **2011**, *2011* (28), 4369−4376.
(54) Chen, N. Y.; Garwood, W. E. Industrial Application of Shape-Selective Catalysis. *Catalysis Reviews* **1986**, *28* (2−3), 185−264.
(55) Ding, H.; Liu, H.; Chu, W.; Wu, C.; Xie, Y. Structural Transformation of Heterogeneous Materials for Electrocatalytic Oxygen Evolution Reaction. *Chem. Rev.* **2021**, *121* (21), 13174−13212.
(56) Konnerth, H.; Matsagar, B. M.; Chen, S. S.; Prechtl, M. H. G.; Shieh, F.-K.; Wu, K. C.-W. Metal-Organic Framework (MOF)-Derived Catalysts for Fine Chemical Production. *Coord. Chem. Rev.* **2020**, *416*, No. 213319.
(57) Ye, G.; Wan, L.; Zhang, Q.; Liu, H.; Zhou, J.; Wu, L.; Zeng, X.; Wang, H.; Chen, X.; Wang, J. Boosting Catalytic Performance of MOF-808(Zr) by Direct Generation of Rich Defective Zr Nodes via a Solvent-Free Approach. *Inorg. Chem.* **2023**, *62* (10), 4248−4259.
(58) Timofeeva, M.; Panchenko, V.; Jun, J.; Hasan, Z.; Matrosova, M.; Jhung, S. Effects of Linker Substitution on Catalytic Properties of Porous Zirconium Terephthalate UiO-66 in Acetalization of Benzaldehyde with Methanol. *Applied Catalysis A: General* **2014**, *471*, 91−97.
(59) Herbst, A.; Khutia, A.; Janiak, C. Brønsted Instead of Lewis Acidity in Functionalized MIL-101Cr MOFs for Efficient Heterogeneous (Nano-MOF) Catalysis in the Condensation Reaction of Aldehydes with Alcohols. *Inorg. Chem.* **2014**, *53* (14), 7319−7333.
(60) Gupta, S. K.; Zuniga, J. P.; Abdou, M.; Thomas, M. P.; De Alwis Goonatilleke, M.; Guiton, B. S.; Mao, Y. Lanthanide-Doped Lanthanum Hafnate Nanoparticles as Multicolor Phosphors for Warm White Lighting and Scintillators. *Chemical Engineering Journal* **2020**, *379*, No. 122314.
(61) Balme, G.; Gore, J. Conversion of Acetals and Ketals to Carbonyl Compounds Promoted by Titanium Tetrachloride. *J. Org. Chem.* **1983**, *48* (19), 3336−3338.

https://doi.org/10.1021/acsomega.4c05760
ACS Omega 2024, 9, 37386−37395